

## Article

# Kinetic and Isotherm Studies for Cu<sup>2+</sup> and Cs<sup>+</sup> Uptake with Mono- and Bimetallic FeO(OH)-MnOx-Clinoptilolite

Eva Chmielewska \* , Marek Bujdoš, Marek Hupian  and Michal Galamboš 

Faculty of Natural Sciences, Comenius University, Ilkovičova 6, Mlynská Dolina, 842 15 Bratislava, Slovakia; marek.hupian@uniba.sk (M.H.)

\* Correspondence: eva.chmielewska@uniba.sk; Tel.: +421-260296410

**Abstract:** This study investigates the adsorption of selected water pollutants, namely caesium and copper, by using natural zeolite of the clinoptilolite type, as well as clinoptilolites coated with MnOx, FeO(OH)-MnOx and FeO(OH). A comprehensive evaluation of these processes was conducted. The kinetics of Cs and Cu adsorption on all examined samples smoothly followed the pseudo-second-order kinetic model, with the liquid film step regarded as the slower step in both cases. The Langmuir isotherm model provided the most accurate description of Cs and Cu adsorption for all examined samples. However, when considering natural clinoptilolite and FeO(OH)-clinoptilolite systems in relation to Cu(II), the Redlich–Peterson model slightly outperformed the Langmuir model. The modification of clinoptilolite with Mn and Fe oxyhydroxides did not significantly enhance the removal efficiency of Cs compared to the unmodified sample. In contrast, the adsorption capacity, especially for MnOx-clinoptilolite, increased fourfold for Cu and other tested cations such as Pb and Zn, indicating improved efficiency in these cases.

**Keywords:** Mn and Fe oxyhydroxides zeolite; Cs(I); Cu(II) adsorption



**Citation:** Chmielewska, E.; Bujdoš, M.; Hupian, M.; Galamboš, M. Kinetic and Isotherm Studies for Cu<sup>2+</sup> and Cs<sup>+</sup> Uptake with Mono- and Bimetallic FeO(OH)-MnOx-Clinoptilolite. *Minerals* **2023**, *13*, 1536. <https://doi.org/10.3390/min13121536>

Academic Editors: Davide Comboni, Concetta Rispoli, Dario Fancello, Marco Lezzerini and Stefano Columbu

Received: 17 October 2023  
Revised: 4 December 2023  
Accepted: 6 December 2023  
Published: 11 December 2023



**Copyright:** © 2023 by the authors. Licensee MDPI, Basel, Switzerland. This article is an open access article distributed under the terms and conditions of the Creative Commons Attribution (CC BY) license (<https://creativecommons.org/licenses/by/4.0/>).

## 1. Introduction

Copper ranks as the third most abundant metal element in the human body, following iron and zinc [1–3]. There are a total of 29 copper isotopes, with Cu-63 constituting approximately 69% of naturally occurring isotopes. Caesium-137 is a radioactive isotope of caesium generated as a common fission product during the nuclear fission of uranium-235 and other fissionable isotopes in nuclear reactors and nuclear weapons. It emerges as one of the most challenging fission products to handle, due to its short-to-medium half-life (30 years) [4–12]. Caesium-137 was released into the environment during nearly all nuclear weapon tests and certain nuclear accidents, notably the abovementioned Chernobyl and Fukushima Daichii disasters [6,13–16]. Not only major accidents, but also numerous minor incidents contribute to the radioactive contamination of our environment according to the literature published under [3–6,8,9,17,18].

In recent years, substantial efforts have been invested into designing water treatment methods for removing hazardous metals from water. Among the recommended techniques like chemical precipitation, ion exchange, membrane filtration, coagulation–flocculation and adsorption, adsorption is undoubtedly one of the most economically viable and effective methods in water technology [8–15]. Adsorption is also considered one of the most suitable methods for final water purification, owing to its simplicity and the availability of various natural or commercial adsorption materials [16–30]. Over the last decade, nanomaterials-based zeolite-type mesoporous adsorbents have garnered attention in the scientific community for removing hazardous metal pollutants, including radionuclides. Their improved adsorption ability and selectivity are based mainly on the organic ligand complexation with target ions [23–27,31,32]. In the case of an ion exchange separation of Cs, inorganic ion exchangers are found to be superior over organic ion exchangers due to

their thermal stability, resistance to ionising radiation and good compatibility with final waste forms. Therefore, several clay minerals, including montmorillonite, illite and others, have also been applied for the removal of radioactive contaminants [8–10,19–22,28,31]. While natural zeolites have traditionally been used for removing Cs-137 from low- and intermediate-level radioactive waste effluents, a drawback lies in the competitive interactions of other monovalent cations, particularly Na and K in waste effluents, which can considerably lower Cs adsorption [8,9,22,31]. Transition metal hexacyanoferrates, particularly nickel hexacyanoferrate, (Prussian blue analogue) is known to be highly selective for caesium adsorption and has been regarded as the most promising adsorbent in terms of selectivity and capacity for caesium ions [8–10,13,18]. Recently, coir pith, or highly functionalised mangrove charcoal, has emerged as a promising candidate adsorbent for removing radioactive ions from aqueous solutions as well [15–17,21,28].

This study aims to evaluate the fundamental and key data of Cu(II) and Cs-137 adsorption by using the monometallic FeO(OH)- and MnOx-coated, as well as bimetallic FeO(OH)-MnOx-coated, clinoptilolites originating from Slovakia. The review primarily focuses on the kinetics of Cu<sup>2+</sup> and Cs-137 uptake from aqueous solutions using four different calculation models: the pseudo-first-order kinetic model according to Lagergren; the pseudo-second-order kinetic model according to Ho and McKay; the intraparticle diffusion model according to Weber and Morris; and the liquid film diffusion model. The adsorption equilibrium data were characterised using two-parameter empirical adsorption isotherm models according to Langmuir, Freundlich and BET, as well as the three-parameter model according to the Redlich–Peterson isotherm.

## 2. Experimental Section

### 2.1. Adsorption Materials Examined

The physicochemical specification of the inland clinoptilolite examined in this study, including structure and the surface morphology, is published in the literature [33]. The clinoptilolite used in this research comes from a long-term mined surface deposit near Nižný Hrabovec, from the region of East Slovak neovolcanites. The mineralogical composition of the Slovak zeolite rock, as referred elsewhere [33–35], is the following: clinoptilolite 70%–80%, volcanic glass 15%–20%, feldspar 7%–10%, cristobalite 2%–4% and alfa-quartz 2%–3%. The MnOx-clinoptilolite, obtained in the form of crushed and sifted rock with an initial grain size ranging from 0.2 to 1.0 mm, was prepared following the procedure outlined in reference [33]. The preparation method involved an almost semi-operational process, conducted at ambient temperature and by maintaining a neutral pH. This process needed a larger volume of chemicals, including 5% KMnO<sub>4</sub> and 30% MnSO<sub>4</sub> solutions. The resulting MnOx-clinoptilolite served as the starting material for the synthesis of a combined bimetallic FeO(OH)-MnOx zeolite. The other monometallic FeO(OH)-zeolite was synthesised in a relatively lower amount by using a laboratory equipment and following the procedure published in [33]. 20 g of (0.2–1.0 mm) grain-sized zeolite was mixed with 0.5 L of 10% aqueous solution of iron(III) nitrate nonahydrate (Fe(NO)<sub>3</sub>·9H<sub>2</sub>O; Alfa Aesar, Crystalline, Germany) and left to mature at 60 °C in a laboratory water bath shaking machine for 3 days. Subsequently, a 200 mL solution of 2.5 M KOH was slowly added to achieve a final suspension with a pH of 12. This mixture was further aged for almost one week at room temperature. Following the completion of the reaction and the addition of all chemicals, the suspension underwent filtration using a cellulose membrane paper (KA 4, Fisher Scientific, Peršejn, Czech Republic) for qualitative analysis. The filtered material was then washed with deionised water (electrolytic conductivity less than 0.20 μS/cm) and finally dried at 105 °C for 2 h in a laboratory dryer.

The mono- and bimetallic Fe and Mn oxide-supported clinoptilolite was thoroughly characterised with thermoanalytical FT-IR, XRD, SEM and XPS spectroscopy. All the spectral procedures that were used confirmed the occurrence of a new MnO<sub>2</sub> phase (predominantly birnessite), including mostly amorphous iron oxy(hydr)oxide, i.e., FeO(OH) species on the surface of the above-synthesised adsorbents as published under [33–35]. An

average SEM-EDS composition of natural zeolite of clinoptilolite type and its 3 modified samples are present in Table 1 and in the study [34].

**Table 1.** Specific surface areas and porosity values of the adsorbents studied.

Sample	Grain Size	S <sub>BET</sub> (m <sup>2</sup> /g)	S <sub>t</sub> (m <sup>2</sup> /g)	V <sub>micro</sub> (cm <sup>3</sup> /g)
Slovak natural zeolite of clinoptilolite type	0.2–0.6 mm	31.7	21.4	0.004
Slovak natural clinoptilolite	≤20 μm	59.2	-	
FeO(OH)–MnOx-clinoptilolite of Slovak origin	≤100 μm	31.4	28.8	0.001
MnOx–Slovak clinoptilolite	≤100 μm	27.5	22.9	0.002
FeO(OH)-clinoptilolite of Slovak origin	≤100 μm	52.2	38.2	0.007

S(BET)—Surface area determined via nitrogen adsorption and BET isotherm. S(t)—Surface area of mesopores plus external surface area determined via t plot method. V(micro)—Volume of micropores determined via t plot method.

## 2.2. Batch Adsorption Experiments

Batch mode or discontinuous adsorption experiments for basic adsorbent characterisation (system equilibrium setup and adsorption isotherm calculations) were carried out according to the conventional method reported elsewhere [10–12,21–27], as follows: A 30 mL of solution, measured with analytical precision, of different initial concentrations, together with 0.3 g of adsorbent, weighed to 4 decimal places, were added into resealable plastic vials and mixed using rotation mode for the selected time at constant speed (180 rpm) on a Biosan SIA Multi-rotator in order to reach equilibrium. The aqueous solutions obtained through a 0.45 μm cellulose membrane filtration were analysed. A powdered grain size fraction less than 0.2 mm for all adsorbent samples was used. All measurements were made in triplicate at a laboratory temperature of 23 ± 0.2 °C. The equilibrium uptake capacity  $a_{eq}$  in mg/g for each sample was calculated according to the following mass balance Equation (1):

$$a_{eq} = \left( \frac{C_i - C_{eq}}{m} \right) V \quad (1)$$

where  $c_i$  and  $c_{eq}$  are initial and equilibrium concentrations of the pollutant studied (in mg/L),  $m$  is the mass of the adsorbent examined (in g) and  $V$  is the volume of the solution in litres (L). The stock solution of CuSO<sub>4</sub> (purum), prepared in acidified deionised (D.I.) water with pH = 4.5, was purchased from Lachema Brno (made in the Czech Republic). Stock solutions of caesium were prepared by dissolving the grade reagent CsCl of analytical purity in acidified deionised (D.I.) water (pH = 4) and enriched with low level activity (<sup>137</sup>Cs was used as a tracer for analysis). The radioindicator <sup>137</sup>Cs was supplied by the National Centre for Nuclear Research POLATOM (Otwock, Poland). CsCl was purchased from AnalaRBDH chemicals Ltd., Poole, England.

## 2.3. Analytical Methods

The copper content of the solutions was determined via flame atomic absorption spectrometry at 324.7 nm and a 0.7 nm slit, with deuterium background correction (AAS Model 1100, Perkin Elmer, Waltham, MA, USA). Calibration standards were prepared from Cu 1000 mg/L stock solution (CertiPUR, Merck, Germany). The measurement range was 0.05–10 mg/L; the solutions with higher Cu concentration were diluted.

The adsorption of Cs-137 onto zeolite was performed via the radioisotope indication method using a radioisotope Cs-137 as referred in [36]. Parameters affecting adsorption were examined by adding 5 mL of aqueous solution to 0.05 g of zeolite in a plastic tube in order to minimise the radioactive waste produced. Zeolite and aqueous solutions were mixed in a rotary laboratory mixer with a constant mixing speed. Subsequently, the suspension was centrifuged at 8000 rot/min for 15 min and an aliquot of each supernatant

was collected and analysed using a Modumatic model gamma spectrometer equipped with a NaI(Tl) detector. The best initial pH for the highest Cs adsorption on zeolite was determined at pH = 4 from among the scales of 1 up to 10 and the influence of contact time on adsorption capacity was studied from 1 min up to 420 min.

For the characterisation of the material and structural investigation of the samples, the external surface area and porosity of the clinoptilolite rock, including competitive samples, were determined at liquid nitrogen temperature (76 K) in a Micromeritics ASAP 2400 apparatus, using the static volumetric technique and t plot methods with the BJH pore diameter computation.

### 3. Results and Discussion

#### 3.1. Kinetic Studies

First, the kinetic measurements presented in Figure 1 were performed to distinguish the Cu(II) and Cs-137 removal performance of the three selected adsorbents. The data at all curves (Figure 1) refer to the arithmetic average values of three parallel measured samples, usually for every time interval until the equilibrium. The study of Cu(II) adsorption dependence with time onto various zeolites was carried out for solutions with  $C_0 = 399$  mg/L and the original pH value 4.5, as well as the study of Cs-137 with a solution concentration of  $C_0 = 500$  mg/L and pH = 4. Due to the more or less overlapping of the resulting adsorption capacities towards Cs-137 for all, i.e., the kinetic and isotherm curves, among the MnOx-, FeO(OH)-MnOx- and the natural zeolite, only one selected measurement for natural zeolite versus Cs-137 solution was chosen for plotting. The experimental kinetic data obtained (Figure 2, Table 2) were calculated using the OriginLab Corp. ORIGINPro v 9.1 (Data Analysis and Graphing Software 2013).

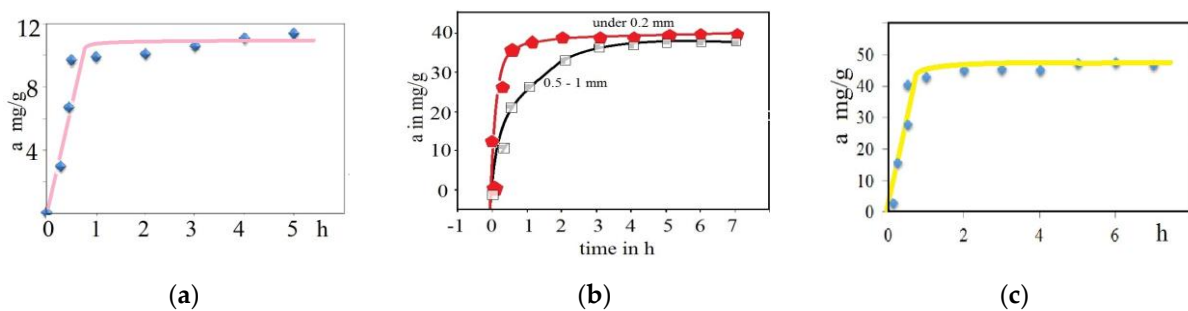


**Figure 1.** Kinetics for Cu(II) removal on the (a) natural and (b) MnOx-zeolite with 2 various grain size fractions (natural zeolite was in powdered form less than 0.2 mm); Cs-137 removal on the (c) natural zeolite.

**Table 2.** Kinetic models for Cu(II) and Cs-137 adsorption onto various samples of zeolite.

Sample Type	$a_{eq}$	$a_{eq}$ mg/g (cal.)	$K_1$ (1/min)	$R^2$	$K_2$ (g/mg·min)	$a_{eq}$ mg/g (cal.)	$R^2$	$K_i$ (g/mg·min <sup>-1/2</sup> )	$K_{fd}$ (mg/g·min <sup>-1</sup> )
	mg/g (exp.)	Pseudo	First	Order	Pseudo	Second	Order	Intraparticle Diffusion	Liquid Film Diffusion
MnOx-zeolite grain size less than 0.2 mm/Cu(II)	39.4	3.6	0.00186	0.93396	0.00709	39.7	0.99998	0.23125	0.00984
MnOx-zeolite 0.5–1.0 mm/Cu(II)	37.8	24.7	0.00271	0.95596	0.00090	40.6	0.99903	1.21873	0.0123
Natural zeolite less than 0.2 mm/Cu(II)	11.6	3.1	0.00151	0.88450	0.00609	11.9	0.99726	0.14631	0.00763
Natural zeolite less than 0.2 mm/Cs-137	48.0	7.1	0.00564	0.83985	0.00239	48.3	0.99903	0.42684	0.00592

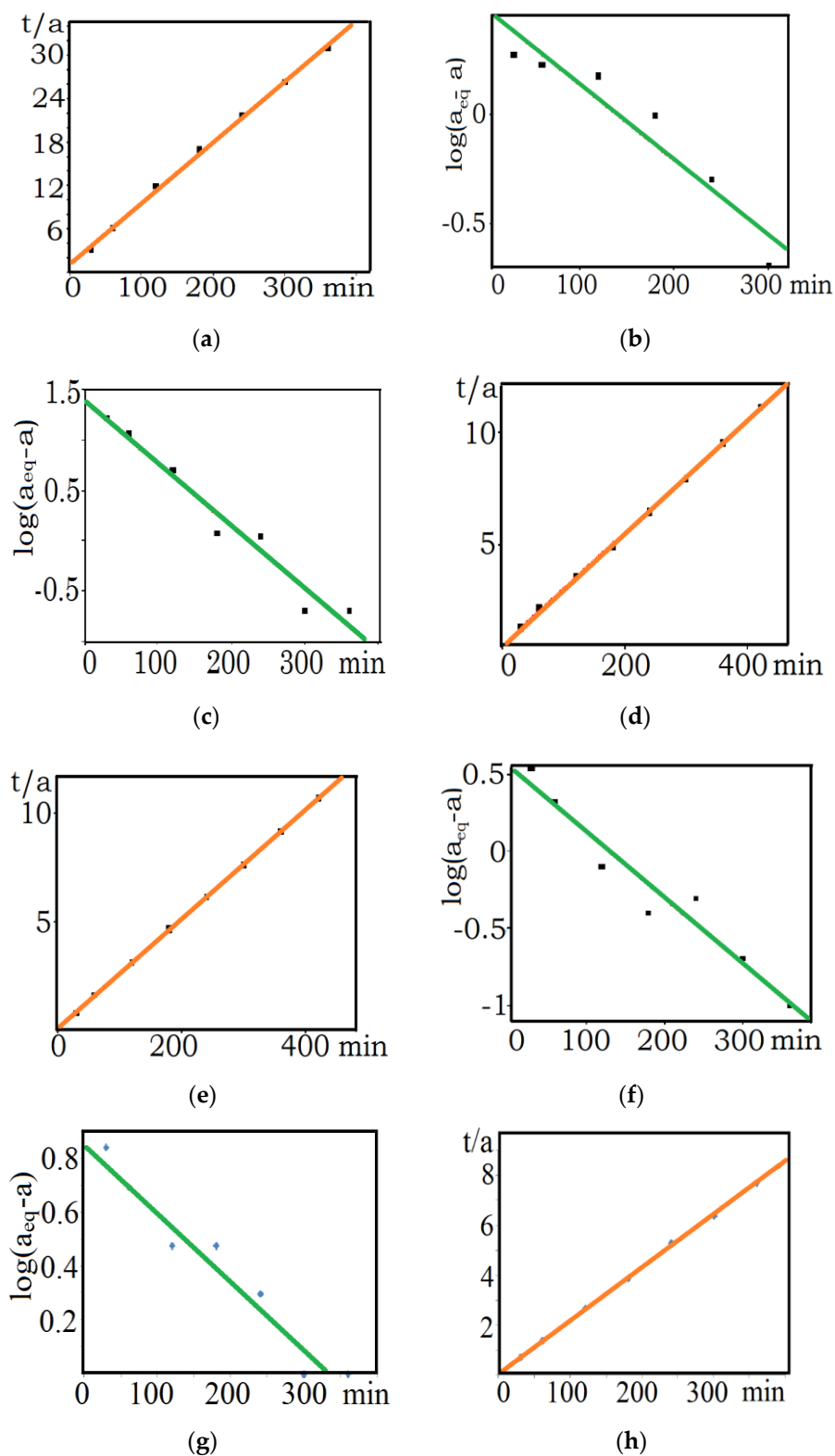


**Figure 2.** Pseudo-second-order kinetic model for Cu(II) adsorption on (a) natural zeolite with less than 0.2 mm grain size, (d) MnOx-zeolite with 0.5–1 mm grain size, (e) MnOx-zeolite with less than 0.2 mm grain size and (h) for Cs-137 adsorption on natural zeolite. Pseudo-first-order kinetic model for Cu(II) adsorption on (b) natural zeolite with less than 0.2 mm grain size, (c) MnOx-zeolite with 0.5–1 mm grain size, (f) MnOx-zeolite with less than 0.2 mm grain size and (g) for Cs-137 adsorption on natural zeolite.

The kinetics of  $\text{Cu}^{2+}$  and  $\text{Cs}^+$  uptake from aqueous solutions were evaluated using four different calculation models: the pseudo-first-order kinetic model according to Lagergren (2), the pseudo-second-order kinetic model according to Ho and McKay (3), the intraparticle diffusion model according to Weber and Morris (4) and the liquid film diffusion model (5) [32,37]:

$$\log(a_{\text{eq}} - a) = \log a_{\text{eq}} - \frac{k_1}{2.303}t \quad (2)$$

$$\frac{t}{a} = \frac{1}{k_2 a_{\text{eq}}^2} + \frac{1}{a_{\text{eq}}}t \quad (3)$$

The adsorbate can diffuse into the interior of the porous adsorbent particles while intraparticle diffusion can be described using Equation (4):

$$a = k_i \sqrt{t} + C \quad (4)$$

where  $k_1$ ,  $k_2$  and  $k_i$  are the pseudo-first-order, pseudo-second-order rate constants and the rate parameter of the intraparticle diffusion control stage, respectively;  $a_{\text{eq}}$  is the maximum amount of solute adsorbed at equilibrium in mg/g;  $a$  is the amount of solute on the surface of the adsorbent at any time  $t$  in mg/g and  $C$  is the intercept at the ordinate. The overall rate of adsorption is controlled by the most slow step, which used to be either film or pore diffusion. When the transport of adsorbate from the liquid phase up to the solid phase boundary plays the most significant role in adsorption, the liquid film diffusion model (5) may be applied:

$$\ln(1 - F) = -k_{\text{fd}} \cdot t \quad (5)$$

where  $F$  is the fractional equilibrium ( $F = a_t/a_{\text{eq}}$ ) and  $k_{\text{fd}}$  is the adsorption rate constant. A linear graph— $\ln(1 - F)$  versus  $t$  with zero intercept—may suggest that the kinetics of the adsorption process is controlled by diffusion through the liquid film surrounding the solid adsorbent.

As depicted in Table 2, it is evident that all the systems examined in this study can be characterised in terms of kinetics following the pseudo-second-order model. Notably, the most time-consuming step in this process appears to be the diffusion through the liquid film.

### 3.2. Isotherm Studies

Furthermore, the determination of the adsorption capacity at various equilibrium concentrations is used to be plotted as an experimental adsorption isotherm. Table 3 and Figure 3 present the adsorption results on various surface-modified zeolite samples, including the natural one using the statistical regression analysis (Origin version 9.1E, Origin Lab Corp. Linear Fit, Burlington, NC, USA). The equilibrium data from Figure 3 were analysed via two-parameter empirical adsorption isotherm models Langmuir (6), Freundlich (7) and BET (8), as well as with the three-parameter Redlich–Peterson isotherm (9). Results are listed in Table 3:

$$\frac{1}{a} = \left( \frac{1}{a_{\text{max}} \cdot b \cdot c_{\text{eq}}} \right) + \left( \frac{1}{a_{\text{max}}} \right) \quad (6)$$

$$a = K \cdot c_{\text{eq}}^{\frac{1}{n}} \quad a = \log K + \frac{1}{n} \log c_{\text{eq}} \quad (7)$$

$$\frac{c_{\text{eq}}}{a(c_{\text{sat}} - c_{\text{eq}})} = \frac{1}{K_{\text{BET}} \cdot a_{\text{max}}} + \frac{K_{\text{BET}} - 1}{K_{\text{BET}} \cdot a_{\text{max}}} \cdot \frac{c_{\text{eq}}}{c_{\text{sat}}} \quad (8)$$

$$a = \frac{A \cdot c_{\text{eq}}}{1 + B \cdot c_{\text{eq}}^g} \quad \ln\left(A \frac{c_{\text{eq}}}{a} - 1\right) = g \ln c_{\text{eq}} + \ln B \quad (9)$$

where  $a$  means the specific adsorption capacity in mg/g;  $a_{max}$  is the maximum adsorption capacity in mg/g;  $c_{eq}$  is the equilibrium concentration in solution in mg/L;  $b$  relates to the affinity of the solute for the binding sites expressed in L/mg;  $c(sat)$  means saturation concentration in solution in mg/L;  $K_{F,L,BET}$  are coefficients of individual isotherms in L/mg;  $n$  means a heterogeneity factor of Freundlich isotherm (without unit) and  $A, B$  and  $g$  are nonlinear regression constants of the Redlich–Peterson isotherm.

**Table 3.** Langmuir, Freundlich, BET and Redlich–Peterson isotherm data for Cu(II) adsorption by using natural, FeO(OH)-, FeO(OH)-MnOx- and MnOx-zeolite and for Cs-137 adsorption by using natural zeolite.

Adsorbent/ Adsorbate	Langmuir Isotherm			Freundlich Isotherm		BET Isotherm		Redlich–Peterson Isotherm				
	$a_{max}$ mg/g	$a_{max}$ mg/g	$a_{max}$ mg/g	$n$	$K_F$ L/mg	$R^2$	$K_{BET}$ L/mg	$R^2$	$g$	$A$ L/g	$B$ (L/mg)g	$R^2$
MnOx-zeolite/Cu(II)	60.97	0.0351	0.9995	5.7372	18.8191	0.9312	−13.2438	0.8621	0.4240	2.2782	0.7814	0.7164
FeO(OH)-MnOx-zeolite/Cu(II)	35.34	0.0048	0.9836	5.5710	7.4611	0.9708	−6.2651	0.8271	0.6170	63.0545	0.4746	0.9218
FeO(OH)-zeolite/Cu(II)	17.89	0.0048	0.9725	4.2230	2.6669	0.9127	−1.7427	0.7220	0.7811	2.8011	0.3246	0.9841
Natural zeolite/Cu(II)	17.24	0.0104	0.9896	4.8733	3.6392	0.9297	−1.8110	0.5848	0.8474	2.7475	0.1899	0.9951
Natural zeolite/Cs-137	119.33	0.0159	0.9965	1.9981	4.2459	0.9577	3.7671	0.2034	0.1899	1.8087	1.6084	0.6077

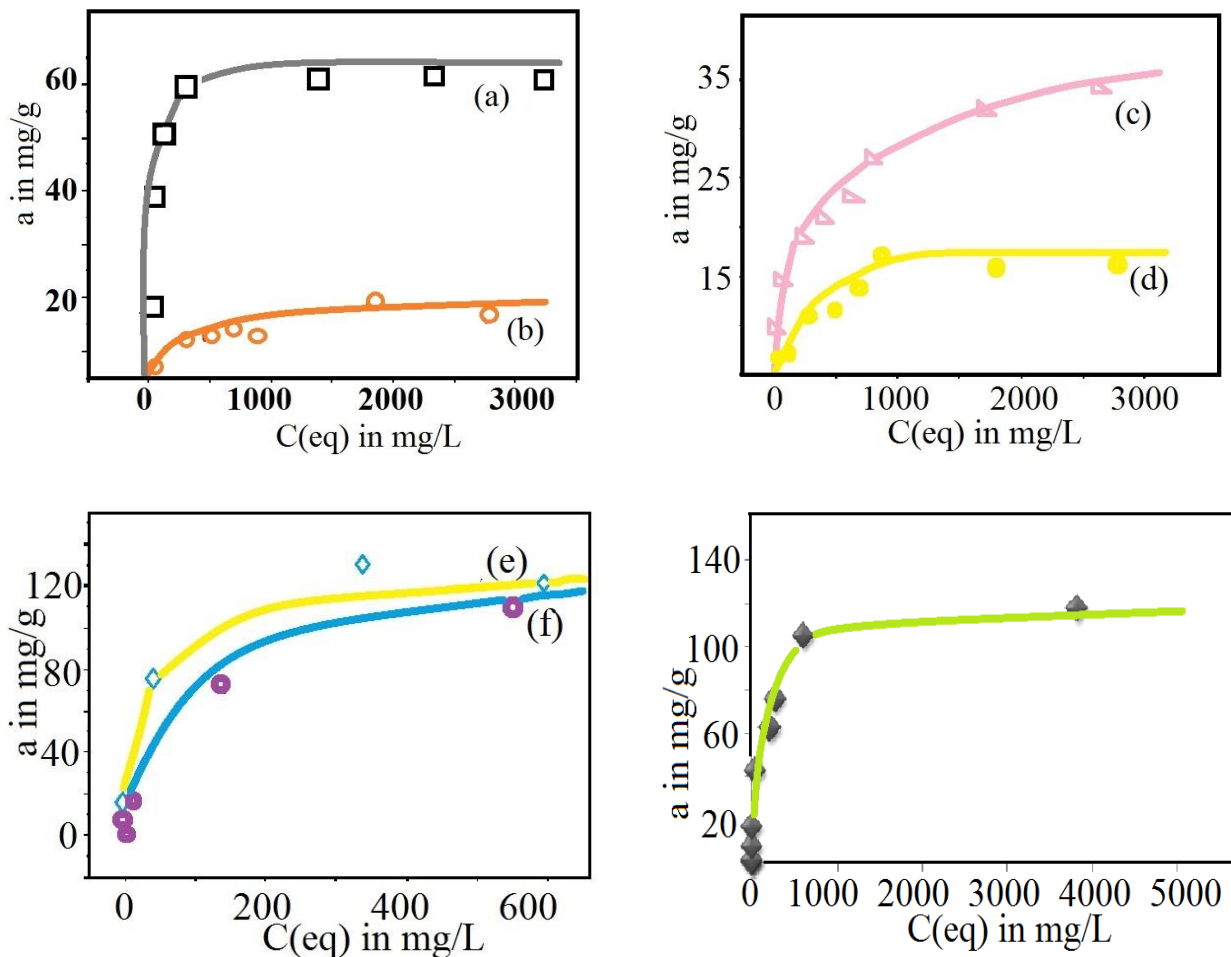


**Figure 3.** Experimental adsorption isotherms at  $23 \pm 0.2$  °C for (a) MnOx-zeolite, (b) natural zeolite, (c) FeO(OH)-MnOx-zeolite, (d) FeO(OH)-zeolite versus Cu(II) solution and (e) FeO(OH)-MnOx-zeolite, (f) MnOx-zeolite, (lower right) natural zeolite versus Cs-137 solution.

From the calculations performed and graphical plotting of the experimental results, it emerged that, based on the determination coefficients  $R^2$ , the validity of the Langmuir isotherm clearly prevails almost for all of the systems studied. Only both systems of natural zeolite and FeO(OH)-zeolite versus Cu(II) were slightly better described with the Redlich–Peterson model (Figure 3, Table 3). The polymolecular two-parameter empirical BET isotherm model resulted in the least fitted one. Furthermore, from Table 3 and the calculated adsorption capacities, it can be deduced that the clinoptilolite modified with Mn and Fe oxyhydroxides did not improve Cs-137 removal efficiency in that extent, as was the case by the simple ion-exchanged clinoptilolite; however, by Cu and other previously tested Pb and Zn cations, the capacity, especially of MnOx-zeolite, increased approximately fourfold in regard to natural zeolite [31,33]. For FeO(OH)-MnOx-treated clinoptilolite in the Cu, Pb and Zn cation solutions, the adsorption capacity in regard to the natural zeolite samples was only recorded with doubled high values. It may be assumed that iron and manganese oxyhydroxides penetrated into the pore structure of the zeolite surface and changed the properties of the surface, but did not block accessibility for Cs-137 to migrate into the internal zeolite structure; they enabled Cs-137 to easily—and without any restriction—penetrate inside the zeolite matrix, through equilibrium attainment however, and thus was time-dependent. The embedding of nanodispersed FeO(OH) hydrogels and various manganese oxides into mainly microporous and mesoporous structures of clinoptilolite rock considerably decreased the  $S_{\text{BET}}$  values of these products, except for the FeO(OH)-clinoptilolite, whose  $S_{\text{BET}}$  value remained only slightly lower in regard to the untreated original rock (Table 1). The graphical comparison of pore size distribution for all chemically treated zeolite samples is shown in Figure 4. According to Table 1, the natural zeolite was characterised with the lowest surface area of mesopores, including external surface area ( $S_t$  is approximately 2/3 of the total  $S_{\text{BET}}$ ), while the Mn and Fe oxyhydroxide-coated zeolite samples contained higher values of  $S_t$  in regard to their  $S_{\text{BET}}$ . The highest volume of micropores  $V_{\text{micro}}$  was confirmed by FeO(OH)-clinoptilolite and the lowest by FeO(OH)-MnOx-clinoptilolites and MnOx-clinoptilolite, which could indicate that the MnOx components may preferentially incorporate into the micropores. These results support the following assumptions: Slovak clinoptilolite rock preferentially adsorbs Cs-137 into its micropores (pore dimensions of clinoptilolite are  $3.3 \times 4.6 \text{ \AA}$ ,  $3.0 \times 7.6 \text{ \AA}$  and  $2.6 \times 4.7 \text{ \AA}$  [35]), while zeolite surface covering with Mn(IV) and Fe(III) oxyhydroxides might suppress Cs-137 migration into its structure. This was clearly shown by the equilibrium measurements (adsorption efficiency versus time dependence), where the natural zeolite already reached equilibrium in 2 h, but chemically treated FeO(OH)-MnOx-zeolite only in 7 hrs. The results from previous investigations of Cs adsorption onto Slovak clinoptilolite, i.e., onto the natural and Na<sup>+</sup>-exchanged one, referred to the adsorption capacity of 249.6 mg/g for Na<sup>+</sup>-exchanged clinoptilolite compared to approximately 100 mg/g for the natural clinoptilolite (Table 5) [31]. This considerable increase in the removal efficiency of Na<sup>+</sup>-exchanged clinoptilolite may be explained by cleaning and by the release of the internal porous space of the clinoptilolite during the chemical ion exchange treatment and replacement of the original mixture of ions (K, Ca, Mg, Na [35]) with Na cations, which are more thermodynamically suitable for its dimension size (radius of hydrated Na cation is 3.58 Å with  $-\Delta H = 420 \text{ kJ/mol}$ , radius of hydrated K cation is 3.3 Å with  $-\Delta H = 340 \text{ kJ/mol}$ , radius of hydrated Ca cation is 4.1 Å with  $-\Delta H = 1615 \text{ kJ/mol}$  and radius of hydrated Mg cation is 4.3 Å with  $-\Delta H = 1960 \text{ kJ/mol}$ ) [36,38]. Nevertheless, it may be supposed that a large, poorly hydrated Cs ion (its radius of hydrated ion is 5.05 Å and  $-\Delta H = 280 \text{ kJ/mol}$  only) will release some of the water molecules or it may be deformed or flattened through the migration into the zeolite structure by exchange with Na ions. In our current research, the Cs-137 removal efficiency onto the examined natural, MnOx and FeO(OH)-MnOx-zeolites was more or less similar, which supports the above clarified phenomenon of a higher priority of Cs ion towards micropores. Some interesting results of a similar study were achieved by Voronina et al. [8,9,31], who compared the adsorption capacity of Russian natural and by ferrocyanide-modified clinoptilolites, while finding

almost no difference in the capacities of both samples. Their capacity values correspond well with our capacity values for Cs-137 uptake, despite another surface functionalisation. Tables 4 and 5 illustrate the lists of some selected adsorption materials used for Cu and Cs ion uptake, published in the scientific literature, in order to compare our capacity values for Cu and Cs ion uptake with those found by the foreign authors. From Table 4, it can be seen that Stojakovic et al. [22] obtained a similar capacity value as in our case (17 mg/g) for Cu(II) ion uptake onto natural zeolite; however, the manganese oxide clinoptilolite from Iran reached the maximum capacity towards Cu(II) at only 6.9 mg/g, which, in regard to our measured maximum capacity of 60 mg/g, means that it is one order of magnitude lower in value [25,32].

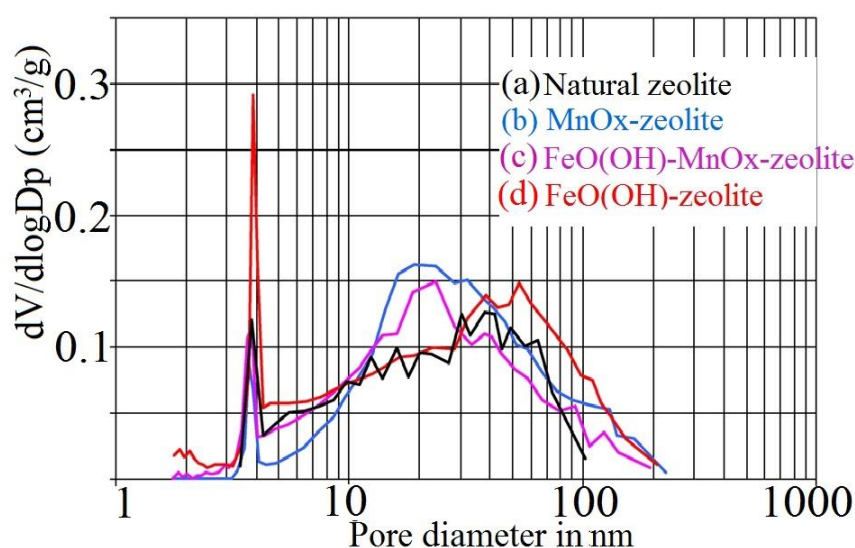


**Figure 4.** Comparison of pore size distribution of (a) natural zeolite of clinoptilolite type, (b) MnOx-zeolite, (c) FeO(OH)-MnOx-zeolite and (d) FeO(OH)-zeolite.

**Table 4.** The literature review of maximum adsorption capacities to Cu(II) for some adsorbents.

Adsorbent	Max. Adsorption Capacity in mg/g to Cu(II)	Reference in This Study
Coconut seed powder (CCP)	4.3	[21,28]
Sesame seed cake powder (SSCP)	4.2	[28]
Ground nut seed cake powder (GNCSP)	4.8	[15,28]
Shells of lentil (LS)	9.6	[15,21]
Wheat (WS)	17.4	[17,21]
Rice (RS)	2.9	[21]
Iron oxide-clinoptilolite, Iran	8.8	[24,25]
Manganese oxide-clinoptilolite, Iran	6.9	[25,32]
Natural zeolite (clinoptilolite), Zlatokop, Serbia	16.8	[22]
CTAB—surfactant-coated kaolin	38.5	[19,20]
Natural kaolin	19.2	[21,28]
Sewage sludge ash (SSA)	4.1	[30]
Pectin-coated iron oxide magnetic nanocomposite adsorbent	49.0	[29]
ZnO <sub>2</sub> nanoparticles green synthesised with Aloe vera	20.4	[27]
Elemental selenium nanoparticles	890	[26]
TiO <sub>2</sub> nanosorbent	9.3	[23]

**Table 5.** The literature review of maximum adsorption capacities to Cs(I) on some adsorbents.

Adsorbent	Max. Adsorption Capacity in mg/g to Cs(I)	Reference in This Study
Prussian Blue encapsulated alginate/calcium beads	142.8	[18]
Prussian Blue analogue on chitosan/carbon nanotubes	219.8	[8–10]
Polyacrylonitrile–K–Ni–Cyanoferrates	157.7	[18]
Zirconium molybdopyrophosphate	183.4	[14]
Dibenzo-30-crown-10-ether immobilised mesoporous adsorbent	107.2	[13]
Fly ash-based geomaterials	89.3	[10,13]
K <sub>1.93</sub> Ti <sub>0.22</sub> Sn <sub>3</sub> S <sub>6.43</sub> adsorbent	450.1	[11]
Opaline mudstone	32.1	[12]
Slovak natural clinoptilolite	99.8	[31]
Na-exchanged Slovak clinoptilolite	249.6	[31]
Russian natural clinoptilolite	135	[8,9]
Russian ferrocyanide-modified clinoptilolite	136	[8,9]
Ferrocyanide-modified silica gel	53.2	[13]
Ammonium-pillared montmorillonite/CoFe <sub>2</sub> O <sub>4</sub> -Ca-alginate	86.5	[19]
Lignocellulosic coir pith with nickel hexacyanoferrate	93.3	[15–17]
Mangrove charcoal-modified adsorbent	133.5	[15,16]

The radius of 4.19 Å of the hydrated copper cation, with its  $-\Delta H = 2084$  kJ/mol, is considered comparable to the more likely examined Pb cation (radius of hydrated ion is 4.01 Å and  $-\Delta H = 1496$  kJ/mol) and Zn cation (radius of hydrated ion is 4.3 Å and  $-\Delta H = 2080$  kJ/mol), which is consistent with its mutual adsorption behaviour [38]. Usually, at a low pH solution, a positive charge prevails on the surface of the hydrated oxides. Most literary sources and their authors classify Fe(III) oxyhydroxides as anion active or exchangeable anions, that is, oxides with a positive charge on the surface, while the surface of MnOx is an cation active or is cation exchanging, that is, with a negative charge [33]. This statement is in good agreement with our results, because a negatively charged MnOx-zeolite showed the highest Cu, Zn and Pb ion uptake capacity, while the FeO(OH)-zeolite with a positive surface charging showed the lowest adsorption ability for those cations. Considering the achievement of a fourfold higher adsorption capacity for the studied Pb, Zn and Cu ions, compared to the natural zeolite, we can assume that zeolite coated with manganese polyoxides externally and partially internally works as a parallel adsorbent [31,33]. All of the above ions from solutions probably mechanically intercalate between the parallel layers of manganese oxides (inner sphere complex adsorption), which is especially typical for the manganese oxide structure of birnessite [33] and likely also occurs on the zeolite surface (Table 3).

#### 4. Conclusions

Zeolites are favoured as ion exchange materials for effectively removing radionuclides, particularly Cs-137 and Sr-90, from aqueous nuclear wastes due to their well-established highly selective ion exchange characteristics and cost-effectiveness. They also effectively adsorb heavy metal cations. In the present study, adsorptive capabilities of unmodified and various modified clinoptilolites with regard to selected water contaminants, namely caesium and copper, were investigated using batch adsorption technique, under static experimental conditions at ambient laboratory temperature. Pseudo-second-order kinetic model proved to be the best option for the abovementioned cations' adsorption onto clinoptilolites. While the Langmuir isotherm adsorption model provided a better description of Cs and Cu adsorption, the Redlich–Peterson model presented better results for natural and FeO(OH)-clinoptilolites systems. While the adsorption capacity for Cu and other previously tested cations like Pb and Zn increased approximately fourfold, especially with MnOx-zeolite, compared to natural zeolite, the capacity for Cs remained nearly unchanged. This result underscores the continued preference for using natural clinoptilolite in the removal of radiocaesium from aqueous solutions or from radioactive wastes.

**Author Contributions:** Conceptualization E.C.; methodology E.C., M.H. and M.G.; software E.C.; validation E.C., M.B., M.H. and M.G.; formal analysis, E.C., M.H. and M.G.; investigation E.C.; resources E.C.; data curation, E.C. and M.B.; writing—original draft preparation E.C.; writing—review and editing, E.C., M.H. and M.G.; visualization E.C.; supervision E.C.; project administration E.C., M.B., M.H. and M.G.; funding acquisition M.H. and M.G. All authors have read and agreed to the published version of the manuscript.

**Funding:** This research was funded by Science and Scientific Grant Agency VEGA, Project No. 1/0356/23.

**Data Availability Statement:** The authors declare that all analytical data supporting the findings of this study are available within the paper or cited in peer-review references.

**Conflicts of Interest:** The authors declare no conflict of interest.

## References

1. Rowshanfarzada, P.; Sabetb, M.; Reza Jaliliana, A.; Kamalidehghan, M. An overview of copper radionuclides and production of  $^{61}\text{Cu}$  by proton irradiation of nat. Zn at a medical cyclotron. *Appl. Radiat. Isot.* **2006**, *64*, 1563–1573. [[CrossRef](#)] [[PubMed](#)]
2. Johnson, M.D.; Larry, E. (Eds.) “Copper”. *Merck Manual Home Health Handbook*; Merck Sharp & Dohme Corp., a Subsidiary of Merck & Co., Inc.: Gujarat, India, 2008; Archived from the Original on 7 March 2016.
3. Copper, Chemical Element—Overview, Discovery and Naming, Physical Properties, Chemical Properties, Occurrence in Nature, Isotopes. Available online: <http://www.chemistryexplained.com/elements/C-K/Copper.html> (accessed on 16 October 2023).
4. Haynes, W.M. (Ed.) *CRC Handbook of Chemistry and Physics*, 95th ed.; CRC Press/Taylor and Francis: Boca Raton, FL, USA, 2015.
5. Coursey, J.S.; Schwab, D.J.; Tsai, J.J.; Dragoset, R.A. *Atomic Weights and Isotopic Compositions*; Version 4.1; National Institute of Standards and Technology: Gaithersburg, MD, USA, 2015.
6. George, L.; Trigg Immergut, E.H. *Encyclopedia of Applied Physics, Vol. 4: Combustion to Dimagnetism*; VCH Publishers: Hoboken, NJ, USA, 1992; pp. 267–272.
7. Delacroix, D.; Guerre, J.P.; Leblanc, P.; Hickman, C. *Radionuclide and Radiation Protection Handbook*; Nuclear Technology Publishing: Ashford, UK, 2002.
8. Voronina, A.V.; Kulyaeva, I.O.; Gupta, D.K. Determination of parameters of selective  $^{137}\text{Cs}$  sorption onto natural and ferrocyanide–modified glauconite and clinoptilolite. *Radiochem* **2018**, *60*, 35–41. [[CrossRef](#)]
9. Voronina, A.V.; Yu, N.A.; Semenishchev, V.S.; Gupta, D.K. Decontamination of seawater from  $^{137}\text{Cs}$  and  $^{90}\text{Sr}$  radionuclides using inorganic. *Sorbents J. Environ. Radioact.* **2020**, *217*, 106–210. [[CrossRef](#)]
10. Zhang, H.; Zhu, M.; Du, X.; Feng, S.; Miyamoto, N.; Kano, N. Removal of Cesium from Radioactive Waste Liquids Using Geomaterials. *Appl. Sci.* **2021**, *11*, 8407. [[CrossRef](#)]
11. Jiang, Z.; Liu, G.; Ma, C.; Guo, Y.; Duo, J.; Li, M.; Deng, T. Cesium removal from wastewater: High-efficient and reusable adsorbent  $\text{K}_{1.93}\text{Ti}_{0.22}\text{Sn}_3\text{S}_{6.43}$ . *Chemosphere* **2022**, *305*, 135406. [[CrossRef](#)] [[PubMed](#)]
12. Kwon, S.; Kim, Y.; Roh, Y. Effective cesium removal from Cs-containing water using chemically activated opaline mudstone mainly composed of opal-cristobalite/tridymite (opal-CT). *Sci. Rep.* **2021**, *11*, 15362. [[CrossRef](#)] [[PubMed](#)]
13. Awual, R. Ring size dependent crown ether based mesoporous adsorbent for high cesium adsorption from wastewater. *Chem. Eng. J.* **2016**, *303*, 539–546. [[CrossRef](#)]
14. Lv, K.; Xiong, L.-P.; Luo, Y.-M. Ion exchange properties of cesium ion sieve based on zirconium molybdopyrophosphate. *Colloids Surf. A Physicochem. Eng. Asp.* **2013**, *433*, 37–46. [[CrossRef](#)]
15. Ofomaja, A.E.; Pholosi, A.; Naidoo, E.B. Application of raw and modified pine biomass material for cesium removal from aqueous solution. *Ecol. Eng.* **2015**, *82*, 258–266. [[CrossRef](#)]
16. Hasan, M.N.; Shenashen, M.A.; Hasan, M.M.; Znad, H.; Awual, M.R. Assessing of cesium removal from wastewater using functionalized wood cellulosic adsorbent. *Chemosphere* **2021**, *270*, 128668. [[CrossRef](#)]
17. Parab, H.; Sudersanan, M. Engineering a lignocellulosic biosorbent—Coir pith for removal of cesium from aqueous solutions: Equilibrium and kinetic studies. *Water Res.* **2010**, *44*, 854–860. [[CrossRef](#)] [[PubMed](#)]
18. Wang, J.; Zhuang, S.; Liu, Y. Metal hexacyanoferrates-based adsorbents for cesium removal. *Coord. Chem. Rev.* **2018**, *374*, 430–438. [[CrossRef](#)]
19. Jiménez-Castañeda, M.E.; Medina, D.I. Use of Surfactant-Modified Zeolites and Clays for the Removal of Heavy Metals from Water. *Water* **2017**, *9*, 235. [[CrossRef](#)]
20. Ab Hamid, N.H.; bin Mohd Tahir, M.I.; Chowdhury, A.; Nordin, A.H.; Alshaikh, A.A.; Suid, M.A.; Nazaruddin, N.I.; Nozaizeli, N.D.; Sharma, S.; Rushdan, A.I. The Current State-of-Art of Copper Removal from Wastewater: A Review. *Water* **2022**, *14*, 3086. [[CrossRef](#)]
21. Aydina, H.; Buluta, Y.; Yerlikaya, C. Removal of copper (II) from aqueous solution by adsorption onto low-cost adsorbents. *J. Environ. Manag.* **2008**, *87*, 37–45. [[CrossRef](#)] [[PubMed](#)]
22. Stojakovic, D.; Milenkovic, J.; Daneu, N.; Rajic, N. A Study of the Removal of Copper Ions from aqueous solution using Clinoptilolite from Serbia. *Clays Clay Miner.* **2011**, *59*, 277–285. [[CrossRef](#)]

23. Ezati, F.; Sepehr, E.; Ahmadi, F. The efficiency of nano TiO<sub>2</sub> and γ Al<sub>2</sub>O<sub>3</sub> in copper removal from aqueous solution by characterization and adsorption study. *Sci. Rep.* **2021**, *11*, 18831. [[CrossRef](#)]
24. Dasgupta, S.; Das, M.; Klunk, M.A.; Xavier, S.J.; Caetano, N.R.; Wander, P.R. Copper and chromium removal from synthetic textile Wastewater using clay minerals and zeolite through the effect of pH. *J. Iran. Chem. Soc.* **2021**, *18*, 3377–3386. [[CrossRef](#)]
25. Irannajad, M.; Kamran Haghighi, H.; Soleimanipour, M. Adsorption of Zn<sup>2+</sup>, Cd<sup>2+</sup> and Cu<sup>2+</sup> on Zeolites coated by Manganese and Iron Oxides. *Physicochem. Probl. Min. Process* **2016**, *52*, 894–908.
26. Bai, Y.; Rong, F.; Wang, H.; Zhou, Y.; Xie, X.; Teng, J. Removal of Copper from Aqueous Solutions by Adsorption on Elemental Selenium nanoparticles. *J. Chem. Eng. Data* **2011**, *56*, 2563–2568. [[CrossRef](#)]
27. de O. Primo, J.; Bittencourt, C.; Acosta, S.; Sierra-Castillo, A.; Colomer, J.F.; Jaeger, S.; Teixeira, V.C.; Anaissi, F.J. Synthesis of Zinc Oxide Nanoparticles by Ecofriendly Routes: Adsorbent for Copper Removal from Wastewater. *Front. Chem.* **2020**, *57*, 1790.
28. Pavan Kumar, G.V.; Malla, K.A.; Yerra, B.; Srinivasa Rao, K. Removal of Cu(II) using three low-cost adsorbents and prediction of adsorption using artificial neural networks. *Appl. Water Sci.* **2019**, *9*, 44. [[CrossRef](#)]
29. Gong, J.-L.; Wang, X.-Y.; Zeng, G.-M.; Chen, L.; Deng, J.-H.; Zhang, X.-R.; Niu, Q.-Y. Copper (II) removal by pectin–iron oxide magnetic nanocomposite adsorbent. *Chem. Eng. J.* **2012**, *185–186*, 100–107. [[CrossRef](#)]
30. Pan, S.-C.; Lin, C.-C.; Tseng, D.-H. Reusing sewage sludge ash as adsorbent for copper removal from wastewater. *Res. Conserv. Recycl.* **2003**, *39*, 79–90. [[CrossRef](#)]
31. Chmielewská, E.; Majzlan, J.; Bujdoš, M. Clinoptilolite with surface-enhanced functionality for radionuclide and inorganic pollutants removal. *J. Radioanal. Nucl. Chem.* **2022**, *331*, 3495–3504. [[CrossRef](#)]
32. Taffarel, S.R.; Rubio, J. Removal of Mn<sup>2+</sup> from aqueous solution by manganese oxide coated zeolite. *Miner. Eng.* **2010**, *23*, 1131–1138. [[CrossRef](#)]
33. Chmielewská, E.; Tylus, W.; Bujdoš, M. Study of mono- and bimetallic Fe and Mn oxides supported clinoptilolite for improved Pb(II) removal. *Molecules* **2021**, *26*, 4143. [[CrossRef](#)] [[PubMed](#)]
34. Chmielewská, E.; Tylus, W. A potential refinement of water endangered with Zn-65 onto modified zeolite. *J. Radioanal. Nucl. Chem.* **2021**, *327*, 31–37. [[CrossRef](#)]
35. Chmielewská, E. *Environmental Zeolites and Aqueous Media: Examples of Practical Solutions*; Betham Science Publishers: Sharjah, United Arab Emirates, 2014.
36. Īnan, S.; Kusumkar, V.V.; Galamboš, M.; Viglašová, E.; Roskopfová, O.; Daňo, M. Isotherm, Kinetic, and Selectivity Studies for the Removal of <sup>133</sup>Ba and <sup>137</sup>Cs from Aqueous Solution Using Turkish Perlite. *Materials* **2022**, *15*, 7816. [[CrossRef](#)]
37. Baskan, M.B.; Pala, A. Removal of arsenic from drinking water using modified natural zeolite. *Desalination* **2011**, *281*, 396–403. [[CrossRef](#)]
38. Morris, D.F.C. Ionic radii and enthalpies of hydration of ions. In *Structure and Bonding*; Jørgensen, C.K., Neilands, J.B., Nyholm, R.S., Reinen, D., Williams, R.J.P., Eds.; Springer: Berlin/Heidelberg, Germany, 1969; Volume 6.

**Disclaimer/Publisher's Note:** The statements, opinions and data contained in all publications are solely those of the individual author(s) and contributor(s) and not of MDPI and/or the editor(s). MDPI and/or the editor(s) disclaim responsibility for any injury to people or property resulting from any ideas, methods, instructions or products referred to in the content.